Oxygen-induced surface reconstructions on curved Ag(111)

Cite as: J. Vac. Sci. Technol. A **39**, 053201 (2021); https://doi.org/10.1116/6.0001167
Submitted: 24 May 2021 • Accepted: 23 June 2021 • Published Online: 13 July 2021

Marie E. Turano, Ludo B. F. Juurlink, Maxwell Z. Gillum, et al.

JVST A
Journal of Vacuum Science & Technology A

ARTICLE

avs.scitation.org/journal/jva

Oxygen-induced surface reconstructions on curved Ag(111)

Cite as: J. Vac. Sci. Technol. A **39**, 053201 (2021); doi: 10.1116/6.0001167
Submitted: 24 May 2021 · Accepted: 23 June 2021 ·
Published Online: 13 July 2021

Marie E. Turano,[1] Ludo B. F. Juurlink,[2] Maxwell Z. Gillum,[1] Elizabeth A. Jamka,[1] George Hildebrandt,[1] Faith Lewis,[1] and Daniel R. Killelea[1,a)]

AFFILIATIONS

[1]Department of Chemistry and Biochemistry, Loyola University Chicago, 1068 W. Sheridan Road, Chicago, Illinois 60660
[2]Leiden Institute of Chemistry, Leiden University, P.O. Box 9502, 2300 RA Leiden, The Netherlands

Note: This paper is a part of the Special Collection Commemorating the Career of Pat Thiel.
[a)]**Electronic mail:** dkillelea@luc.edu

ABSTRACT

The adsorption of oxygen and the resultant O-induced surface reconstructions are key components in heterogeneously catalyzed reactions on silver metal surfaces. O uptake and reconstructions on planar Ag(111) are well-characterized, and in this paper, we show that curved Ag(111) features similar O adsorption and reconstructions. Through a systematic scanning tunneling microscope study of a curved Ag(111) single crystal exposed to gas-phase atomic oxygen at a temperature of 525 K, we observed O_{ad} and, upon higher coverages, saw $p(4 \times 4)$ and $p(4 \times 5\sqrt{3})$ reconstructions form on both the A-type and B-type steps. Exposures at low temperatures (< 500 K) resulted in the formation of subsurface oxygen and the appearance of a stripe pattern and amorphous phase on the surface. Upon heating, stable surface reconstructions were formed. Although the geometric arrangement of atoms along the steps were different, A-type and B-type steps formed the same reconstructions. In addition, the B-type steps also saw the formation of several different features atop the oxygen reconstructions.

I. INTRODUCTION

Silver (Ag) catalysts are widespread in industry, particularly, in the partial oxidation reactions of ethylene to ethylene oxide and methanol to formaldehyde.[1–3] For each of these reactions, the efficacy of silver catalysts has been known for quite some time. Originally, for the partial oxidation of ethylene, a mixture of ethylene, air, water, and hydrogen at atmospheric pressure was flowed over powdered silver at a temperature near 500 K.[4,5] Similarly, the basic approach for the production of formaldehyde was developed over a century ago when a mixture of methanol, water, and air was passed through a silver mesh at atmospheric pressure and temperatures over 800 K.[6,7] For both of these reactions, the appropriate temperatures, pressures, and gas compositions were established early on, but continued development of the catalytic material has resulted in increased yield and efficiencies.[8] Over the years, the details of these reaction mechanisms have become standardized.[9–12] However, the actual oxygen species under reaction conditions still remains elusive. By investigating which reconstructions form under what conditions, we may better understand the reactive species participating in partial oxidation reactions.

One oxygen reconstruction thought to play a role in ethylene oxidation is the $p(4 \times 4)$ structure, a common reconstruction of the Ag–O system.[13,14] In the 1970s, Rovida *et al.*[15] observed a $p(4 \times 4)$ low energy electron diffraction (LEED) pattern and proposed a subsequent oxygen surface structure.[15,16]

Following this initial publication, other groups investigated the $p(4 \times 4)$ structure adding to and revising the model.[17–24] By the early 2000s, there was general consensus on the $p(4 \times 4)$ structure, and with the invention of the Scanning Tunneling Microscope (STM), the first images of the $p(4 \times 4)$ reconstruction were obtained.[25] In addition, early DFT studies indicated that the $p(4 \times 4)$ model was the most thermodynamically favorable and most likely the stable phase of O under the conditions of ethylene epoxidation.[13,26] However, upon reinvestigation of the original STM images, a new model was proposed, with the Ag atoms arranged in triangles and O adatoms decorating the edges of the triangles.[27,28] Additional structures were proposed as well including $p(4 \times 5\sqrt{3})$, $c(3 \times 5\sqrt{3})$, and $c(4 \times 8)$ all with

similar atomic arrangements and oxygen coverages to $p(4 \times 4)$.[3,14,27,28]

While these are just a few oxygen structures that may form on the Ag surface,[13] it is still unclear exactly what role O in the reconstructions plays in heterogeneously catalyzed industrial reactions.[11,29] In addition, studies of silver surface reconstructions have been carried out on planar Ag(111) crystals,[15] whereas the surfaces utilized in industrial reactions are commonly high defect density surfaces. Studies have been done on silver clusters,[30] particles,[31] and powders,[32] but the defects of these surfaces are stochastic, and the studies focused on reactivity. Investigation of oxygen reconstruction formation on a silver crystal with well-defined and well-characterized defects has not yet been performed.[33] Determination of which reconstructions primarily form on highly faceted surfaces will help resolve which is the reactive oxygen reconstruction under industrial conditions.

Herein, an STM investigation of O-induced reconstructions formed on a curved Ag(111) single crystal surface with two types of close-packed steps, A-type and B-type, after atomic oxygen (AO) exposure is discussed. Auras and Juurlink specified the crystal shape, size, and orientation as c-Ag(111)$[1\bar{1}0]R31°$.[33] As shown in Fig. 1, the step geometry of A-type steps is a square arrangement of atoms along the step facet, while B-type steps have a triangular arrangement of atoms.[33] We determined that oxygen induced surface reconstructions were very similar on both Ag(111) and curved Ag(111). The initial uptake and onset of reconstruction depended strongly on step geometry.[34] However, once initiated, both sides of the crystal exhibited similar structures, although the B-type steps showed several features atop the O-induced reconstructions not previously reported.

II. EXPERIMENT

Experiments were performed in an ultrahigh vacuum scanning tunneling microscope (UHV-STM) system described previously.[35] The system consisted of two interconnected chambers, a preparation chamber (base pressure of 1×10^{-10} Torr) and an STM chamber (base pressure of 4×11^{-11} Torr). The preparation chamber was equipped with a variety of surface science techniques including a Specs ErLEED 150 with 3000D controller (LEED), a PHI 10–155 Auger Electron Spectrometer (AES), and a Hiden HAL 3F 301 RC quadrupole mass spectrometer (QMS) for temperature programed desorption (TPD) analysis.

The curved Ag(111) crystal (c-Ag(111)) was obtained from Surface Preparation Labs (Zaandam, NL) and described in detail in a previous publication.[36] The 8 mm long c-Ag(111) was cut at a 31° angle from a circular cylindrical crystal and polished to expose the (111) surface at the apex, the B-type steps on one side, and the A-type steps on the other side, as shown in Fig. 1. The STM tip had a range of about 4.3 mm at 35 K, the temperature where images were obtained. This allowed for imaging from about 3 mm off the apex in the B-type step side (+direction) to about 2 mm off the apex in the A-type step side (−direction). Previous characterization of the clean c-Ag(111) single crystal with the STM verified the positional indexing[34] and was used to determine the location of images in this work. The crystal was cleaned using established procedures,[36,37] and cleanliness was verified with LEED and STM.

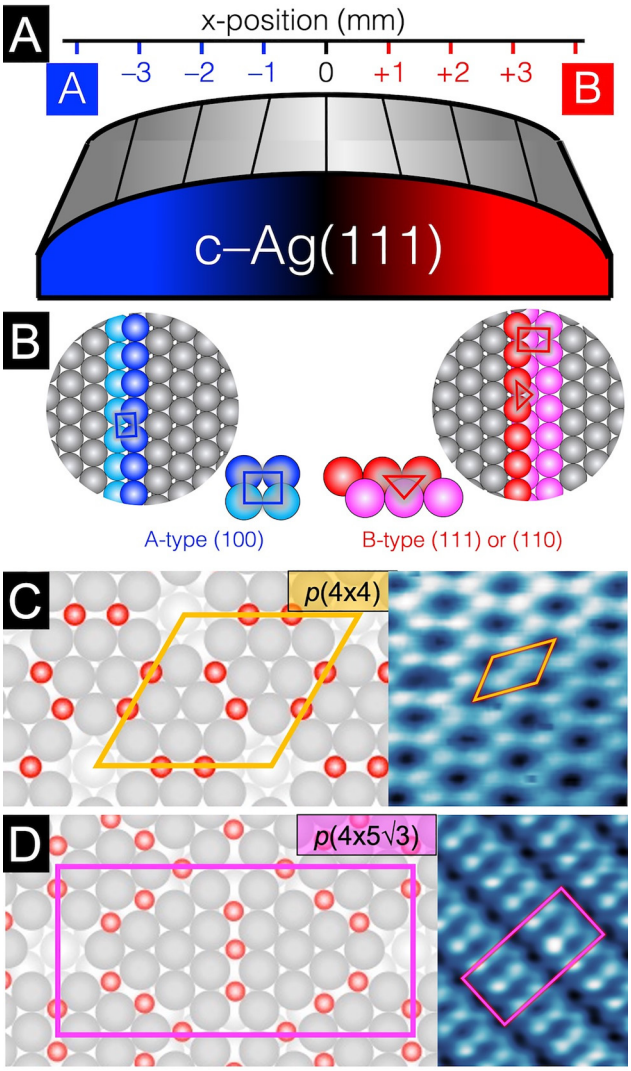

FIG. 1. Depictions of the c-Ag(111) crystal used in this study. (a) Positional indexing in mm across the c-Ag(111) face showing −x values on the A-type step side (blue) and the +x values on the B-type step side (red). (b) Cartoon illustrations showing the step geometries, adapted with permission from Auras and Juurlink, Prog. Surf. Sci. **96**, 100627 (2021). Copyright 2021 Elsevier. Illustrations of two principal O-induced surface reconstructions on Ag(111). (c) The $p(4 \times 4)$ reconstruction unit cell (orange parallelogram) and an STM image and (d) the $p(4 \times 5\sqrt{3})$ reconstruction unit cell (pink rectangle) and an STM image. (c) and (d) Adapted with permission from Derouin *et al.*, ACS Catalysis **6**, 4640–4646 (2016). Copyright 2016 American Chemical Society. (Color version available online).

Atomic oxygen (AO) was generated by backfilling the preparation chamber with O_2 ($P = 5 \times 10^{-7}$ Torr) that was then thermally cracked over a hot Ir filament positioned about 1–2 mm from the front face of the crystal. The atomic oxygen exposure across the crystal face was normal to the top (111) facet. The curvature resulted in modest attenuation of the atomic oxygen flux toward

the edges of the crystal and was uniform on both sides. The crystal was sputtered and annealed to clean between atomic oxygen doses.

The STM chamber housed a Pan Style RHK Scanning Tunneling Microscope with a closed cycle helium cryostat that reached a base temperature of 30 K. All images were taken at 35 K. STM tips were fashioned using the cut and pull technique from 0.25 mm diameter $Pt_{0.8}Ir_{0.2}$ wire. All images were recorded in constant current mode and processed using the Gwyddion software package (http://gwyddion.net). The images used for publication were minimally processed (e.g., cropping, mean plane subtraction or three-point plane subtraction, and/or removal of streaks or blemishes). STM data were used for the determination of chemisorbed oxygen coverage (θ_{Oc}), fraction of reconstruction coverage, and identification of reconstruction phase.

III. RESULTS AND DISCUSSION

The *c*-Ag(111) crystal was exposed to atomic oxygen (AO) at a surface temperature (T_s) of 525 K, where O only sticks as adsorbed oxygen (O_{ad}), to study how the surface structure evolved with varied oxygen coverage. With the configuration used,[14] the flux of O atoms at the crystal face was $(1.2 \pm 0.6) \times 10^{-3}$ monolayers O (ML) s^{-1} (ML is defined with respect to Ag(111); 1 ML $= 1.8 \times 10^{15}$ Ag cm^{-2}), and the day-to-day variations in flux were minor. Exposure durations of 60, 90, 300, 1200, and 2400 s were imaged. The fraction of the surface that reconstructed and the coverage of chemisorbed oxygen (θ_{Oc}) were determined from the STM images obtained directly after each exposure. Previous TPD spectra analysis[34] showed that *c*-Ag and Ag(111) behave similarly in terms of O uptake and desorption.[14,38,39]

Figure 2 shows STM images of *c*-Ag(111) after 60 and 90 s atomic oxygen exposures with $T_s = 525$ K on A-type (color coding blue) and B-type (color coding red) steps. For these conditions, chemisorbed O (O_c) was predominant, and only small patches of reconstruction, primarily $p(4 \times 5\sqrt{3})$, were found on the A-type step side of the crystal. Schnadt *et al.*[40] and Carlisle *et al.*[25] found that O_c appeared as depressions with a diameter of ≈ 1 nm in STM experiments, and a minimum coverage of $\theta_{Oc} = 0.05$ ML was necessary before the onset of reconstruction. The STM images after 60 and 90 s atomic oxygen exposures showed that the O_c depressions had diameters closer to 2 nm. Furthermore, θ_{Oc} was below 0.10 ML for the onset of reconstruction. However, θ_{Oc} was uniform across the crystal for short exposures. STM image analysis depicts that O_c was scattered across the entire crystal surface and previous TPD spectra provided the total oxygen coverage.[34] After a 60 s atomic oxygen exposure, θ_{Oc} was ≈ 0.004 ML, with slightly higher coverages near the apex, where the terraces were largest. From the images in Fig. 2, at the low θ_O coverages after either a 60 s or 90 s exposure, O_c was stochastially scattered across the surface on both the A-type and B-type sides of the crystal, indicating no preferential adsorption under these conditions. After the 60 s atomic oxygen exposure, there were only a few scattered patches of O-induced surface reconstructions along the step edges. As highlighted by the STM images in Figs. 2(a) and 2(b), any reconstructions on the crystal were present only on the A-type steps not the B-type steps.[34]

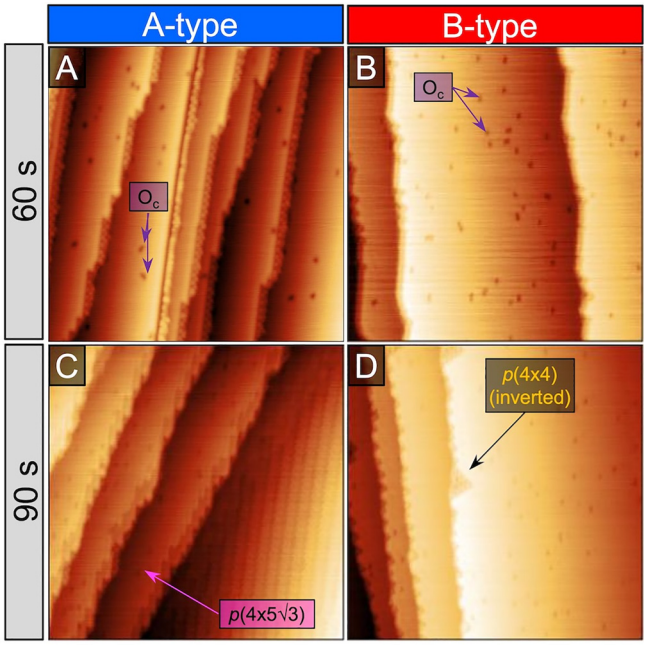

FIG. 2. STM images obtained after short atomic oxygen exposures at $T_s = 525$ K. (a) $x = -1.0$ mm; (b) $x = +1.5$ mm; (c) $x = -0.5$ mm; (d) $x = +1.0$ mm. All images are 56×56 nm^2. Chemisorbed oxygen (O_c) and reconstruction patches are labeled. Imaging conditions are (a) +400 mV, 400 pA; (b) +400 mV, 400 pA; (c) +0.6 V, 400 pA; (d) +0.7 V, 400 pA.

Going from a 60 to a 90 s atomic oxygen exposure, the slight increase in the amount of O on the surface induced more reconstruction formation, as evidenced by the subsequent increase in the fractional coverage of reconstructed oxygen and decrease in chemisorbed O on the surface. The 90 s exposure resulted in some large patches of reconstructions on the surface, occasionally even covering the entire terrace [Figs. 2(c) and 3(b)]. More reconstruction was found at the wider terraces near the apex as opposed to the narrow terraces at the edges of the crystal. The A-type step side had more reconstruction than the B-type step side. At these low coverages, the reconstruction appeared as triangular patches along the step edges, and on the terraces, only the $p(4 \times 5\sqrt{3})$ reconstruction was observed, as was the case for short atomic oxygen exposures on Ag(111).[14] While these triangular features varied slightly in size, most were fairly small. Because the triangles occurred at low coverages, they were likely the precursor to the larger domains of reconstruction, which appeared to grow out of the step edges, as shown in Fig. 3(a). In the upper right-hand corner of Fig. 3(b), the patch of reconstruction was connected to the small triangles along the step edge, suggesting the triangles nucleated the growth of the reconstruction across the terrace. This growth of reconstruction out from the step edge was only observed on the B-type side of the crystal. The A-type side displayed a different reconstruction growth mechanism.[34]

The triangular regions on the B-type steps often showed the $p(4 \times 4)$ reconstruction, but the perimeter was a similar pattern with

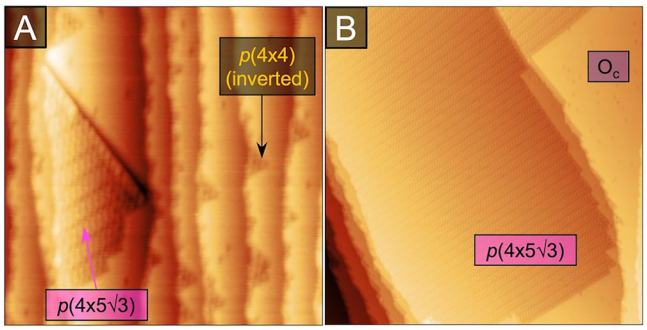

FIG. 3. STM images of 90 s atomic oxygen at $T_s = 525$ K at $x = +0.5$ mm, B-type steps. (a) Triangle reconstruction along the step edges and a larger patch of reconstruction that forms from the initial triangles, 50×50 nm^2; (b) larger patch of reconstruction that almost covers a terrace by growing out of the triangles, 110×110 nm^2. Imaging conditions of both: +0.6 V, 400 pA.

inverted contrast, e.g., a hexagon with dark sides but a bright center, as shown in the STM image in Fig. 4(a). Additionally, smaller patches showed only the inverted $p(4 \times 4)$ pattern, as was reported in a previous publication.[34] We are unsure as to the origin of the inverted contrast shown in Fig. 4, but we have provided line scans to show its periodicity. It could be that these were a result of perturbation to the electronic structure along the border with the metallic area, but electronic structure calculations are needed to provide more insight. Upon closer inspection of this bordering area [STM line profiles in Fig. 4(b)], it is apparent that despite the inverted contrast, the periodicity is the same for both patches. However, the apparent corrugation of the inverted pattern was systematically less than the normal $p(4 \times 4)$ pattern. The inverted contrast pattern was neither observed on the A-type step side of the crystal nor at the interface between two different reconstructions. The inverted pattern was either small isolated patches or along the perimeter of a larger island between the $p(4 \times 4)$ reconstruction and metallic Ag with some O_c.

As the atomic oxygen exposure continued to increase, the surface was increasingly covered by the reconstruction, and the amount of O_c diminished. Both A-type and B-type steps saw an increase in the amount of reconstruction formed, albeit at different rates[34] but the same reconstructions formed on both step types as previously seen on planar Ag(111).

After long atomic oxygen exposures ($\geq$1200 s) to ensure full surface oxidation, new domains of features were observed on the B-type step side of the crystal. Figure 5 shows an STM image taken at $x = +1.5$ mm (B-type steps) that shows a striated phase amid the $p(4 \times 4)$ surface reconstruction. This phase consisted of bright lines spaced about one-half of the $p(4 \times 4)$ surface unit cell. These appear akin to microscopic scratches on the atomic scale, and their origin and identity were unclear. They were never observed on the clean surface and were neither common nor spread over the entire crystal surface but rather were exclusively observed on the B-type side of the crystal.

A second domain, nicknamed the popcorn pattern, was observed after lengthy atomic oxygen exposures ($\geq$1200 s) at $T_s = 525$ K on the B-type steps. Figure 6 shows two STM images of the popcorn pattern decorating bunched steps at $x = +0.75$ mm [Fig. 6(a)] and $x = +0.5$ mm [Fig. 6(b)]. In both images, the $p(4 \times 5\sqrt{3})$ reconstruction appeared interrupted by bright patches, and areas that appear unreconstructed persist on the terraces. As these unreconstructed areas appeared bright, like protrusions, they are unlikely to be oxides. However, they appeared to be of similar

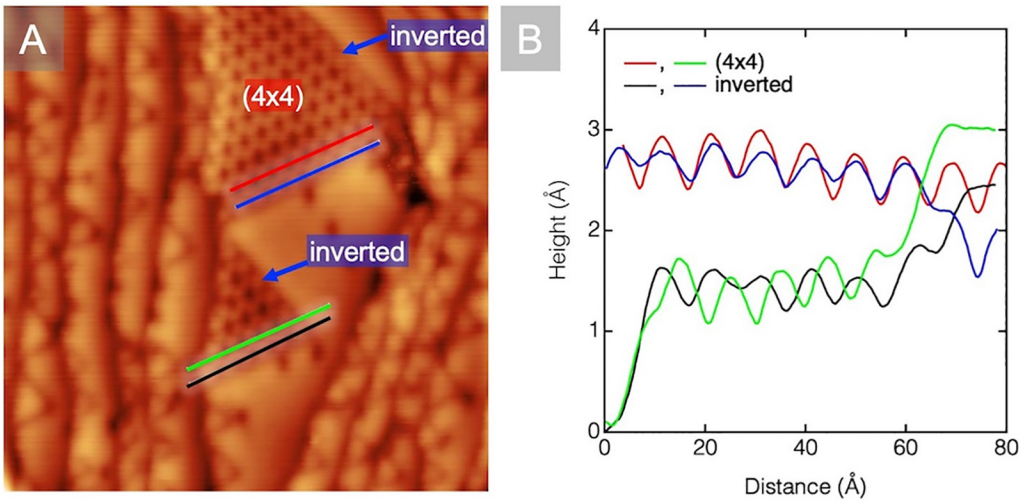

FIG. 4. (a) STM image (26×26 nm^2) at $x = +2.0$ mm on the B-type steps taken after a 1200 s atomic oxygen exposure at $T_s = 525$ K, showing areas of the $p(4 \times 4)$ reconstruction as well as the inverted contrast reconstruction. (b) The plot of the apparent height for line scans from the image in (a) on both the $p(4 \times 4)$ (red, green) and the inverted area (blue, black). The area covered by the line scan indicators was indistinguishable from the portion along the top of the reconstruction. Imaging conditions: +440 mV, 460 pA. (Color version available online).

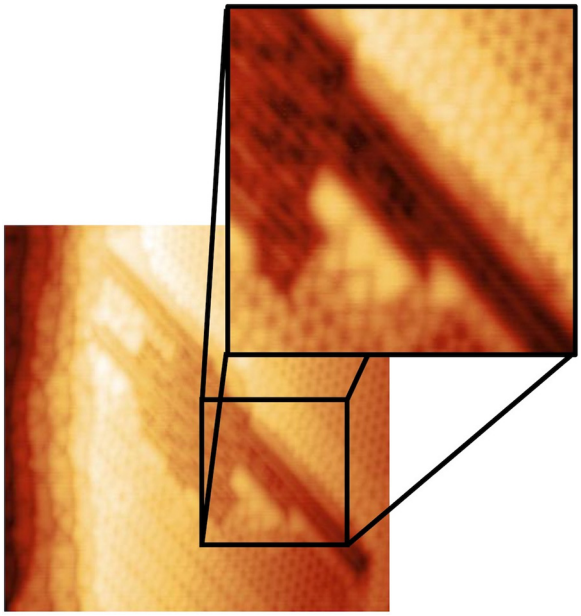

FIG. 5. 40 × 40 nm^2 STM image at x = +1.5 mm (B-type steps) after 1200 s atomic oxygen exposure at T_s = 525 K. The right of the image shows step bunching with limited reconstruction, and the terrace shows a mix of $p(4 \times 4)$ and some $p(4 \times 5\sqrt{3})$ reconstructions, as well as an area of a striated phase. The inset (22 × 22 nm^2) shows the striated phase in greater detail. Imaging conditions: +450 mV, 410 pA.

height in the STM images suggesting they could be akin in composition to the reconstructions. We were unable to resolve these areas in greater detail with STM.

These two different domains were both exclusively on the B-type steps. No different patterns were observed on the A-type step side of the crystal. Reasons for this could be that the closed step geometry on the A-type steps hindered the formation of any different patterns as well as the possibility that the STM could have never managed to image a spot with anything different on the A-type side of the crystal. However, the latter is unlikely since the *c*-Ag(111) was extensively imaged for each atomic oxygen exposure. Each dose required about a week to image the full length of the crystal with ≈500 images per atomic oxygen exposure collected across the face of the crystal. While imaging each dose took a while, the low pressure (≈10^{-11} Torr) and cold temperature (≈35 K) of the STM chamber ensured the surface structures remained stable during imaging and did not decompose.

From the STM images taken at the different positions after varying atomic oxygen exposures and surface temperatures, the fractional coverage of reconstructed areas ($f_{reconstructed}$) and coverage of O_c (θ_{Oc}) was determined and plotted in Fig. 7. The (111) apex and A-type steps had uptake and reconstruction very similar to that observed for Ag(111), with the A-type step side lagging slightly.[34] However, as previously mentioned, it was striking how O uptake and reconstruction were hindered on the B-type step side as the terraces narrowed. In Figs. 7(a)–7(e) (for atomic oxygen exposures from 60 to 2400 s), oxygen uptake and reconstruction formation on the B-type step side of the crystal consistently lagged behind the A-type step side, as previously reported.[34]

The effect of surface temperature during atomic oxygen exposure was also investigated. As previously reported, atomic oxygen exposures for T_s < 500 K resulted in both surface reconstruction and the formation of subsurface oxygen (O_{sub}), with the total

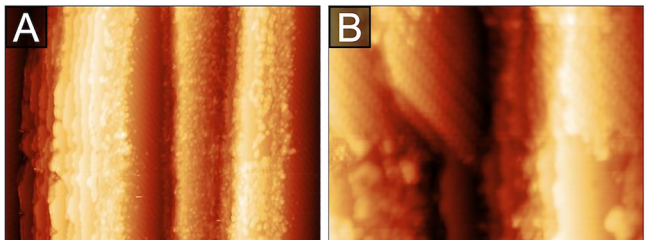

FIG. 6. STM images of *c*-Ag(111) after a 1200 s atomic oxygen with T_s = 525 K showing the popcorn pattern (B-type steps). (a) 170 × 170 nm^2 at x = +0.75 mm, (b) 50 × 50 nm^2 at x = +0.5 mm. Imaging conditions: (a) +470 mV, 410 pA; (b) +470 mV, 410 pA.

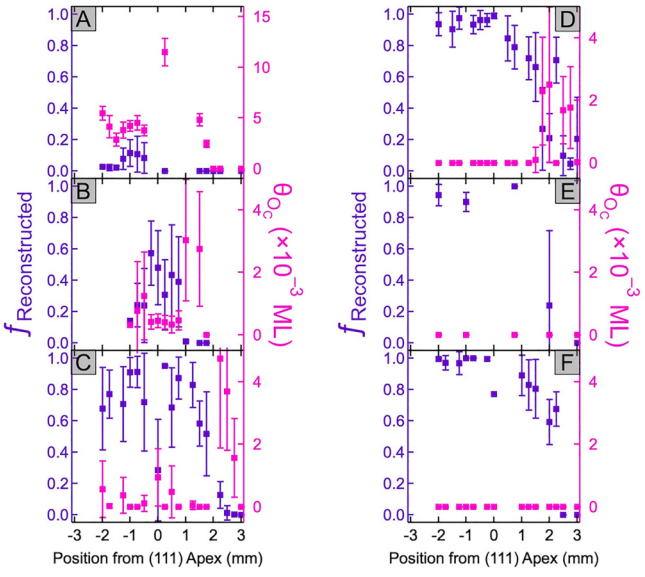

FIG. 7. Fraction of *c*-Ag(111) surface in an O-induced reconstruction ($f_{reconstructed}$, left hand axes, purple) and the apparent coverage of chemisorbed O in unreconstructed areas (θ_{Oc}, right hand axes, pink) after atomic oxygen exposure as a function of position from (111) apex (mm). (a)–(e) for atomic oxygen exposures at T_s = 525 K; (a) 60 s; (b) 90 s; (c) 300 s; (d) 1200 s; (e) 2400 s; and (f) T_s = 450 K, 1200 s. Negative positions correspond to A-type step side of the crystal, positive positions correspond to B-type step side of the crystal.

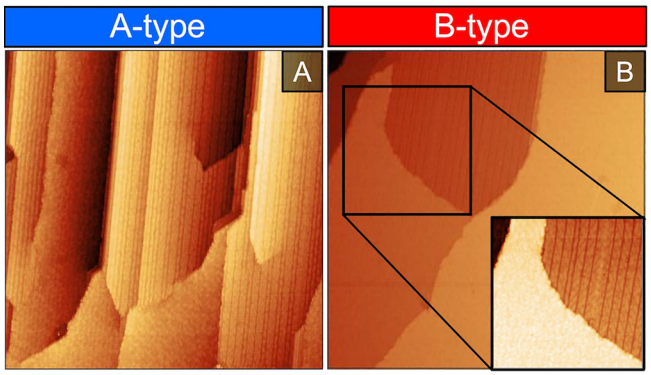

FIG. 8. STM images of *c*-Ag(111) after 1200 s atomic oxygen at $T_s = 450$ K. (a) 140×140 nm^2 image at $x = -0.25$ mm (A-type steps) showing striped and amorphous surface phases as observed on A-type step side of the (111) apex. (b) 140×140 nm^2 image at $x = +1.0$ mm (B-type steps), the inset (56×56 nm^2), showing striped pattern meeting amorphous phase (bright area). Imaging conditions: (a) +0.7 V, 450 pA; (b) +0.9 V, 400 pA; (inset) +0.9 V, 400 pA.

oxygen abundance in excess of the surface oxygen coverage (>0.4 MLO$_{ad}$). The presence of O$_{sub}$ resulted in the formation of a striped phase that uniformly covered the Ag(111) surface.[14,38] Qualitatively, exposure of *c*-Ag(111) to atomic oxygen at $T_s = 450$ K yielded similar results. As shown in Fig. 8, the striped phase was observed, along with an area where structures were not evident and thus have been termed amorphous. Both the A-type steps and the B-type steps displayed these reconstruction patterns which coexisted on the terraces of the crystal and formed due to the presence of O$_{sub}$. There was no preference for step type in the formation of O$_{sub}$. While the A-type steps showed a higher fraction of reconstruction compared to the B-type steps at $T_s = 450$ K [Fig. 7(f)], the striped and amorphous pattern uniformly covered the entire crystal surface. Furthermore, the presence of O$_{sub}$ caused the surface to planarize forming terraces wider than expected at the locations imaged.

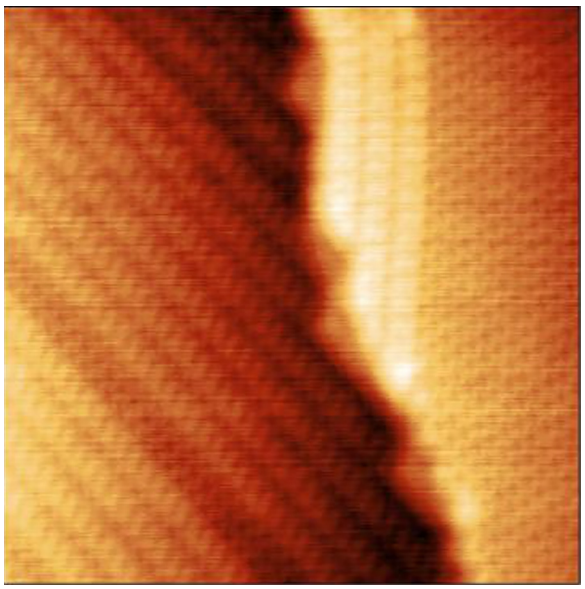

FIG. 9. 56×56 nm^2 STM image of *c*-Ag(111) at $x = +1.25$ mm (B-type steps) obtained after 1200 s atomic oxygen at $T_s = 450$ K and annealed to 525 K for 600 s depicting the common surface reconstructions of Ag(111). Image conditions: +400 mV, 410 pA.

After annealing the $T_s = 450$ K 1200 s atomic oxygen dose to 525 K for 600 s, the surface reverted to the familiar $p(4 \times 4)$ and $p(4 \times 5\sqrt{3})$ structures, indicating that the presence of O$_{sub}$ was responsible for the formation of the stripe and amorphous surface reconstructions. Figure 8 shows STM images taken after 1200 s atomic oxygen dose at $T_s = 450$ K showing the amorphous phase; Fig. 9 shows the same 1200 s atomic oxygen 450 K dose after an anneal at $T_s = 525$ K anneal for 600 s. The $p(4 \times 4)$ and $p(4 \times 5\sqrt{3})$ structures are clearly visible.

IV. CONCLUSION

The quantification, characterization, and identification of O reconstructions on a *c*-Ag(111) crystal were studied. The A-type steps and B-type steps on the *c*-Ag(111) saw the same O reconstructions that form on Ag(111) such as $p(4 \times 4)$ and $p(4 \times 5\sqrt{3})$. Initially, starting with just O$_{ad}$ on the surface, reconstructions gradually begin to form. A-type steps reconstruct at a faster rate than the B-type steps as evidenced by the fact that the fractional reconstruction on the A-type side of the crystal increased much faster than on the B-type side of the crystal. At long atomic oxygen exposures, the steps were fully reconstructed. In addition to familiar structures, the B-type steps also displayed several different patterns atop the reconstructions including a striated pattern and popcorn pattern.

Lower temperature exposures at $T_s = 450$ K still saw the formation of O$_{sub}$ and the formation of the stripe pattern and an amorphous phase. The formation of O$_{sub}$ was not dependent on step geometry as the two aforementioned patterns formed over the entire surface of the crystal. Upon subsequent annealing of the stripe and amorphous patterns, the surface reverted to the commonly seen $p(4 \times 4)$ and $p(4 \times 5\sqrt{3})$ surface reconstructions, showing the thermodynamic stability of the oxygen. Overall, this study showed insight into what reconstructions oxygen forms on different step geometries and the limitations of temperatures and exposure duration.

ACKNOWLEDGMENTS

The authors wish to acknowledge support from the National Science Foundation through Award No. CHE-1800291. M.E.T. thanks The Arthur J. Schmitt Foundation for support during this work. L.B.F.J. thanks the EuroScholars Program for funding a visit to Loyola University Chicago to locally partake in the described experiments and research.

DATA AVAILABILITY

The data that support the findings of this study are available within the article.

REFERENCES

[1]S. Böcklein, S. Günther, and J. Wintterlin, Angew. Chem. Int. Ed. **52**, 5518 (2013).
[2]B. W. Chen, D. Kirvassilis, Y. Bai, and M. Mavrikakis, J. Phys. Chem. C **123**, 7551 (2018).
[3]N. Martin, S. Klacar, H. Gronbeck, J. Knudsen, J. Schnadt, S. Blomberg, J. Gustafson, and E. Lundgren, J. Phys. Chem. C **118**, 15324 (2014).
[4]H. Kestenbaum *et al.*, Ind. Eng. Chem. Res. **41**, 710 (2002).
[5]T. E. Lefort, "Process for the production of ethylene oxide," U.S. patent 1,998,878 (23 April 1935)..
[6]M. D. Thomas, J. Am. Chem. Soc. **42**, 867 (1920).
[7]M. Le Blanc and E. Plaschke, Z. Elektrochem. **17**, 45 (1911).
[8]G. J. Millar and M. Collins, Ind. Eng. Chem. Res. **56**, 9247 (2017).
[9]T. Pu, H. Tian, M. E. Ford, S. Rangarajan, and I. E. Wachs, ACS Catal. **9**, 10727 (2019).
[10]N. Kenge, S. Pitale, and K. Joshi, Surf. Sci. **679**, 188 (2019).
[11]T. E. Jones *et al.*, ACS Catal. **8**, 3844 (2018).
[12]M. Özbek and R. Van Santen, Catal. Lett. **143**, 131 (2013).
[13]A. Michaelides, M. L. Bocquet, P. Sautet, A. Alavi, and D. A. King, Chem. Phys. Lett. **367**, 344 (2003).
[14]J. Derouin, R. G. Farber, M. E. Turano, E. V. Iski, and D. R. Killelea, ACS Catal. **6**, 4640 (2016).
[15]G. Rovida, F. Pratesi, M. Maglietta, and E. Ferroni, J. Vac. Sci. Technol. **9**, 796 (1972).
[16]G. Rovida, F. Pratesi, M. Maglietta, and E. Ferroni, Surf. Sci. **43**, 230 (1974).
[17]A. W. Czanderna, J. Phys. Chem. **68**, 2765 (1964).
[18]H. Albers, W. J. J. Van Der Wal, and G. A. Bootsma, Surf. Sci. **68**, 47 (1977).
[19]G. G. Tibbetts and J. M. Burkstrand, Phys. Rev. B **16**, 1537 (1977).
[20]R. B. Grant and R. M. Lambert, J. Catal. **92**, 364 (1985).
[21]C. T. Campbell, Surf. Sci. **157**, 43 (1985).
[22]S. R. Bare, K. Griffiths, W. N. Lennard, and H. T. Tang, Surf. Sci. **342**, 185 (1995).
[23]A. Raukema, D. A. Butler, F. M. A. Box, and A. W. Kleyn, Surf. Sci. **347**, 151 (1996).
[24]V. I. Bukhtiyarov, V. V. Kaichev, and I. P. Prosvirin, J. Chem. Phys. **111**, 2169 (1999).
[25]C. Carlisle, T. Fujimoto, W. Sim, and D. King, Surf. Sci. **470**, 15 (2000).
[26]W. X. Li, C. Stampfl, and M. Scheffler, Phys. Rev. B **67**, 045408 (2003).
[27]J. Schnadt, A. Michaelides, J. Knudsen, R. T. Vang, K. Reuter, E. Lægsgaard, M. Scheffler, and F. Besenbacher, Phys. Rev. Lett. **96**, 146101 (2006).
[28]M. Schmid *et al.*, Phys. Rev. Lett. **96**, 146102 (2006).
[29]M. Lamoth *et al.*, ChemCatChem **12**, 2977 (2020).
[30]V. I. Bukhtiyarov and V. V. Kaichev, J. Mol. Catal. A: Chem. **158**, 167 (2000).
[31]A. J. F. van Hoof, I. A. W. Filot, H. Friedrich, and E. J. M. Hensen, ACS Catal. **8**, 11794 (2018).
[32]T. C. Rocha, A. Oestereich, D. V. Demidov, M. Hävecker, S. Zafeiratos, G. Weinberg, V. I. Bukhtiyarov, A. Knop-Gericke, and R. Schlögl, Phys. Chem. Chem. Phys. **14**, 4554 (2012).
[33]S. V. Auras and L. B. Juurlink, Prog. Surf. Sci. **96**, 100627 (2021).
[34]M. E. Turano, L. B. F. Juurlink, M. Gillum, E. A. Jamka, and D. R. Killelea, "Structural inhibition of silver surface oxidation," J. Phys. Chem. C (published online 2021).
[35]J. Derouin, R. Farber, and D. Killelea, J. Phys. Chem. C **119**, 14748 (2015).
[36]S. V. Auras, R. A. van Bree, D. L. Bashlakov, R. van Lent, and L. B. Juurlink, Phys. Chem. Chem. Phys. **21**, 15422 (2019).
[37]J. Janlamool, D. Bashlakov, O. Berg, P. Praserthdam, B. Jongsomjit, and L. B. Juurlink, Molecules **19**, 10845 (2014).
[38]M. E. Turano, R. G. Farber, E. C. Oskorep, R. A. Rosenberg, and D. R. Killelea, J. Phys. Chem. C **124**, 1382 (2019).
[39]J. Derouin, R. Farber, S. Heslop, and D. Killelea, Surf. Sci. **641**, L1 (2015).
[40]J. Schnadt *et al.*, Phys. Rev. B **80**, 075424 (2009).